

# Mechanical properties and ablation behaviour of nuclear sacrificial materials containing graphene sulfonate nanosheets

Hong-yan Chu<sup>a,b,\*</sup>, Xiaoli Ge<sup>c</sup>, Jin-yang Jiang<sup>b</sup>, Jinhui Tang<sup>b</sup>, Zhifeng Zhang<sup>b</sup>

<sup>a</sup> College of Civil Engineering, Nanjing Forestry University, Nanjing 210037, China

<sup>b</sup> School of Materials Science and Engineering, Southeast University, Nanjing 211189, China

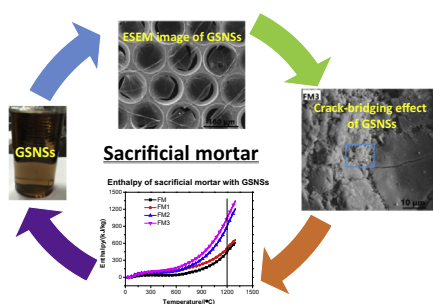
<sup>c</sup> Jiangsu Testing Centre for Quality of Construction Engineering CO., LTD., Nanjing 210028, China



## HIGHLIGHTS

- Mechanical properties and ablation behaviour of sacrificial materials are studied.
- Optimal amount of GSNSs is 0.1 wt% in sacrificial materials.
- Flexural strength of sacrificial mortar increases by 16.22% via GSNSs.
- Compressive strength of sacrificial mortar is up by 24.44% via GSNSs.
- Ablation rate of sacrificial mortar decreases by 50.33% via GSNSs.

## GRAPHICAL ABSTRACT



## ARTICLE INFO

### Article history:

Received 9 June 2018

Received in revised form 10 September 2018

Accepted 2 October 2018

### Keywords:

Sacrificial materials

Ablation behaviour

Graphene sulfonate nanosheets

Microstructure

Mechanical strength

## ABSTRACT

Graphene and its derivatives have been attracting the widespread interest of researchers because of their capability to improve several properties (e.g. mechanical properties, durability, anti-corrosion) of cementitious composites. This paper presents an experimental study on the influence of graphene sulfonate nanosheets (GSNSs) on mechanical properties and ablation behaviour of ferro-siliceous sacrificial cement paste and mortar, including flexural strength, compressive strength, microstructure, porosity, and thermal properties. Based on the results of differential scanning calorimetry and decomposition temperatures, the decomposition enthalpy of ferro-siliceous sacrificial cement paste and mortar was determined. It was found that, (1) the flexural strength and compressive strength of ferro-siliceous sacrificial mortar were increased by 16.22% and 24.44% respectively with the addition of 0.1 wt% GSNSs; (2) the decomposition enthalpy of ferro-siliceous sacrificial mortar was increased by 14.65%, 101.33%, and 135.15%, when adding 0.03 wt%, 0.1 wt%, and 0.3 wt% GSNSs, respectively; (3) the optimum GSNSs content was 0.1 wt% considering the mechanical strength, microstructure, and ablation rate of ferro-siliceous sacrificial cement paste and mortar. These findings can guide the design of ferro-siliceous sacrificial composites, e.g., cement paste, mortar, and even concrete containing GSNSs.

© 2018 Elsevier Ltd. All rights reserved.

## 1. Introduction

At present, cement and concrete composites are the most extensively building and construction materials. However, cementitious composites are quasi-brittle materials and inclined to crack since they have high compressive strength but relatively low flexural strength, and poor strain capacity [1]. Therefore, how to

\* Corresponding author at: College of Civil Engineering, Nanjing Forestry University, Nanjing 210037, China.

E-mail address: [chuhongyan@njfu.edu.cn](mailto:chuhongyan@njfu.edu.cn) (H.-y. Chu).

prevent cracking and improve the tensile strength are the main concerns in the field of cementitious composites [2–4]. Recent progress in nanotechnology provides opportunities to tremendously enhance the performance of cement or concrete composites through nano-sized particles or fibres, such as nano-SiO<sub>2</sub> [5–9], carbon nanotubes [10–15], carbon nano-fibre [15,16], nano-CaCO<sub>3</sub> [17], and nano-TiO<sub>2</sub> [18–20]. Nano-sized materials in cementitious composites are more effective than conventional reinforcements that are usually at millimetre scale, because they can control the formation and development of nano-size cracks at the initial stage [21]. The nanomaterials used in modified cementitious composites can be classified into zero-dimensional (0D) particles (e.g., nano-SiO<sub>2</sub>, nano-TiO<sub>2</sub> and nano-CaCO<sub>3</sub>), one-dimensional (1D) fibres (e.g., carbon nanotubes and carbon nano-fibre), and two-dimensional (2D) sheets according to the shape of nanomaterials.

Graphene and its derivatives, as new 2D nanomaterials, have drawn the most attention in science and engineering in recent years. Graphene has excellent electrical, optical, mechanical, and thermal properties. The average Young's modulus and tensile strength of graphene are 1100 GPa and 125 GPa, respectively [22,23]. The thermal conductivity of suspended graphene is 5300 W/mK [24]. The specific surface area of graphene can theoretically reach  $2.63 \times 10^6$  m<sup>2</sup>/kg [25], which offers more space for physical and chemical interactions between graphene and matrix material. Nevertheless, high production cost and difficulty in dispersing are the major obstacles that limit the application of graphene. As new kinds of nano-sized carbon materials, graphene derivatives (e.g. graphene nanosheets and graphene oxide nanosheets) also contain graphene sheets [26–34], both of which display a 2D sheet-like structure, and the thickness of them is generally less than 10 nm, that is, still at nano scale. Graphene oxide nanosheets (GONSs) are oxides of graphene nanosheets (GNSs), and thus the GONSs have oxygen functional groups that scattered in the 2D sheet-like structure of GONSs. The interaction force between GONSs, namely, van der Waals force can be significantly modified due to the oxygen functional groups, hence the dispersive capacity of GONSs in water can be improved [35]. Shamsaei et al. [36] has summarized the excellent performance of graphene and graphene-based nanosheets, and they point out that graphene and graphene-based nanosheets possess extraordinary mechanical, chemical, thermal and electrical properties, enabling attractive applications, ranging from structural strength/durability improvement, anti-corrosion, to self-cleaning surfaces and energy saving. In addition, the GNSs and GONSs are cheaper to produce than that of graphene.

So far, much research has been done on the effects of GNSs and GONSs on properties of cementitious composites. Ranjbar et al. [37] found that the compressive strength of geopolymer increased by 44%, and that the flexural strength of geopolymer was raised by 116%, respectively, if 1% (mass fraction) GNSs were added. Sun et al. [38] reported that both the flexural and compressive strengths of oil well cement paste were improved because of the addition of GNSs. Du et al. [39] pointed out that the chloride diffusion of concrete was reduced by 80%, when 1.5% of graphene nanoplatelet was added. Mokhtar et al. [40] found that the tensile strength of cementitious composites was enhanced by about 41% due to the addition of 0.03% GONSs. Lv et al. [41] reported that the tensile, flexural and compressive strengths of cementitious composite were increased by 78.6%, 60.7% and 38.9%, respectively, when 0.03 wt% (with respect to weight of cement) GONSs were added. The previous research also indicated that GONSs could regulate the cement hydration process, and further improve the microstructure of cementitious composite [42]. GNSs and GONSs could bring certain self-sensing capability to cementitious composites [30], which was similar to the function of carbon fibre [43]. In

addition, Sha et al. [44,45] suggested that understanding the failure behaviour and failure mechanism of graphene is also important so as to promote its structural and functional applications.

The safety problem of nuclear power is becoming increasingly acute on a global scale. Sacrificial concrete is the hotspot but also a difficulty in the modern nuclear technology. Sacrificial concrete, as a key component of core catcher in nuclear power plant, is designed to prevent leakage of radioactive materials from reactor containment in severe nuclear accident [46]. The corium temperature can be reduced via the interaction between sacrificial concrete and corium. In addition, the physical and chemical properties of the corium can also be modified. Accordingly, the reliability of the core catcher can be improved. As one kind of sacrificial concrete, ferro-siliceous sacrificial concrete is mainly used in the third generation nuclear technology that is the most advanced technique at present. Thermal performance of ferro-siliceous sacrificial concrete, particularly its ablation (erosion of material due to high temperature) behaviour plays a critical role in severe nuclear accident mitigation. Therefore, the ablation behaviour of ferro-siliceous sacrificial concrete should be studied urgently due to the increasing application of ferro-siliceous sacrificial concrete in nuclear power plant. Although graphene and its derivatives have been extensively investigated currently, there is still no available information concerning the effects of graphene sulfonate nanosheets (GSNSs) on microstructure, mechanical properties and ablation behaviour of cementitious composites. The –SO<sub>3</sub>H contained in GSNSs plays a similar role of –OH in GONSs, so the GSNSs may also find their applications in cementitious composites [47]. Furthermore, the total cost of production for GSNSs is about 11% lower than that of GONSs.

The main purpose of the work is to experimentally study the effects of GSNSs on mechanical properties and ablation behaviour of ferro-siliceous sacrificial cement paste and mortar. The flexural strength, compressive strength, thermal analysis, microstructure, porosity, and thermal conductivity of ferro-siliceous sacrificial cement paste and mortar with different contents of GSNSs were comprehensively explored. Based on the experimental results of differential scanning calorimetry and decomposition temperatures, the decomposition enthalpy of ferro-siliceous sacrificial cement paste and mortar was determined. Finally, the ablation behaviour of ferro-siliceous sacrificial cement paste and mortar was investigated in a quantitative manner.

## 2. Experimental program

### 2.1. Materials

P-II 52.5 cement, silica fume, and fly ash (Class I) were utilized in the paper. The chemical composition and physical properties of

**Table 1**  
Chemical composition and physical properties of cement, silica fume, and fly ash.

Materials	Cement	Silica fume	Fly ash
Chemical composition	(wt.%)		
CaO	64.70	0.77	8.38
SiO <sub>2</sub>	20.40	96.18	47.96
Al <sub>2</sub> O <sub>3</sub>	4.70	0.96	30.46
Fe <sub>2</sub> O <sub>3</sub>	3.38	0.85	5.91
MgO	0.87	0.74	2.60
SO <sub>3</sub>	1.88	0.50	1.32
K <sub>2</sub> O	0.83		1.61
Na <sub>2</sub> O			1.76
Loss	3.24		
Physical properties			
Specific gravity	3.15	2.22	
Specific surface (m <sup>2</sup> /kg)	362.20	$2.79 \times 10^4$	
28d Compressive strength (MPa)	62.8		

cement, silica fume, and fly ash are presented in Table 1. Silica sand used in the paper was obtained from a Chinese nuclear industry mineral powders manufacturer, and the silica sand contained, 0.062 wt% MgCO<sub>3</sub>, 0.058 wt.% CaCO<sub>3</sub>, and 99.88 wt% SiO<sub>2</sub>, respectively. Iron ore utilized in the work was provided by the Chinese Nuclear Science and Technology Company, and the chemical constituents of the iron ore were Fe<sub>2</sub>O<sub>3</sub>, SiO<sub>2</sub>, and CaCO<sub>3</sub>, the mass fractions of which were 92.22%, 7.61%, and 0.17%, respectively. The reason for the utilization of silica sand and iron ore is that both SiO<sub>2</sub> and Fe<sub>2</sub>O<sub>3</sub> can oxidize Zr in the corium (a molten mixture of

fuel material). The grading curves of the silica sand and iron ore are shown in Fig. 1. A superplasticizer of polycarboxylate was used to improve the workability of sacrificial cement paste and mortar, and the water-reducing rate of the superplasticizer was 33.9%.

Graphene sulfonate solution was produced and provided by Chinese Graphene Technology Company, and the solid content of the graphene sulfonate solution was 10.5 wt%. In addition, the GSNSs were made as 50–100 μm in diameter and 1–2 nm in thickness. The GSNSs were characterized by SEM, TEM, and FTIR techniques, the results of which are shown in Fig. 2. The elemental composition of GSNSs is presented in Table 2. Note that the elemental composition of GSNSs was analysed by energy dispersive spectrometer (EDS) during SEM experiment, and the result of substrate (Cu) was removed.

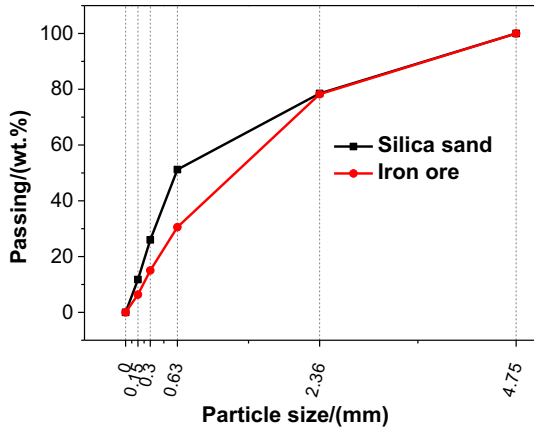


Fig. 1. Grading curves of the silica sand and iron ore.

2.2. Specimen preparation

The mix proportions of ferro-siliceous sacrificial cement paste and mortar used in this work were carefully designed according to our previous research findings, as indicated in literature [48,49]. Based on these results, the mixtures of ferro-siliceous

Table 2  
Elemental composition of GSNSs.

Elements	Weight (wt.%)	Atom (%)	Intensity
C	45.8	59.1	346
O	30.2	29.3	445
S	9.7	4.7	631

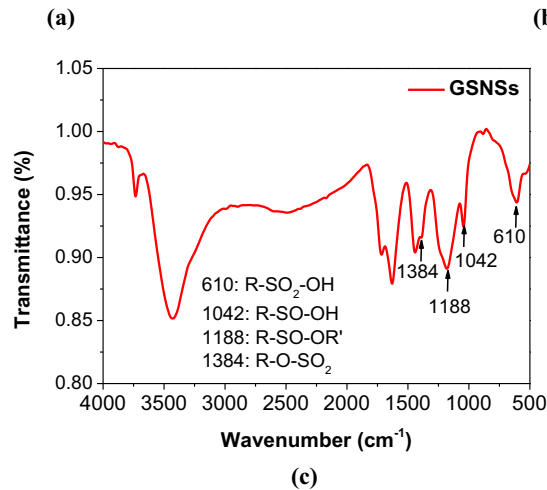
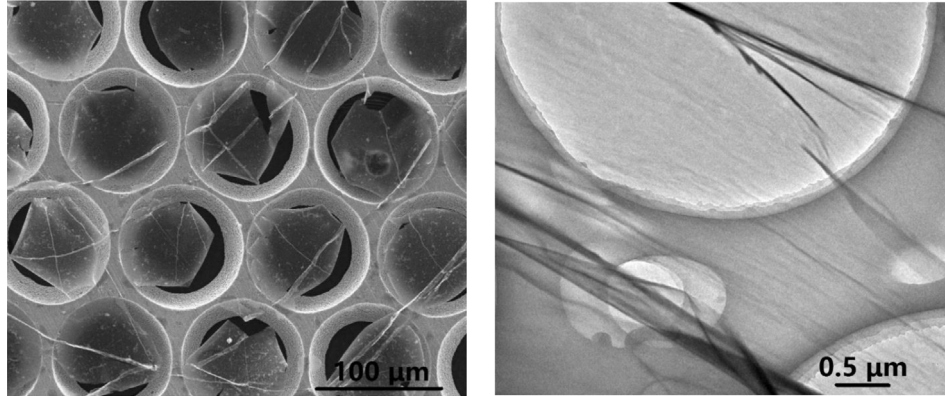


Fig. 2. Material characterization of GSNSs: (a) SEM, (b) TEM, and (c) FTIR.

**Table 3**  
Mix proportions of ferro-siliceous sacrificial cement paste and mortar (g).

	Cement	Fly ash	Silica fume	Silica sand	Iron ore	Water	Superplasticizer	GSNSs
FP	388	135	20	0	0	181	3.8	0
FP1	388	135	20	0	0	181	3.9	0.163
FP2	388	135	20	0	0	181	4.2	0.543
FP3	388	135	20	0	0	181	4.7	1.629
FM	388	135	20	712	917	181	8.0	0
FM1	388	135	20	712	917	181	8.1	0.163
FM2	388	135	20	712	917	181	8.3	0.543
FM3	388	135	20	712	917	181	8.6	1.629

sacrificial cement paste and mortar were further improved through the addition of GSNSs, as presented in Table 3. For convenience, the mixtures of sacrificial cement paste were marked as FP, FP1, FP2, and FP3, and the mixtures of sacrificial mortar were labelled as FM, FM1, FM2, and FM3, which denote different weight fractions of GSNSs 0 wt%, 0.03 wt%, 0.1 wt%, and 0.3 wt%, respectively. It should be noted that the content of GSNSs in the mixtures was calculated by weight of binders (cement, silica fume, and fly ash), and the workability of ferro-siliceous sacrificial cement paste and mortar was kept consistent during their respective preparation process by adding different content of superplasticizer.

According to the aforementioned mix proportions, the specimens (shape: prismatic; size: 40 × 40 × 160 mm) of ferro-siliceous sacrificial cement paste and mortar were cast. The specimens were covered with plastic film after casting. The specimens were cured about 24 h at natural conditions before they were demolded. And then the specimens were cured in a standard curing room for 28 days, and the temperature and relative humidity of the curing room were 21 ± 1 °C and above 95%, respectively. 20 prismatic samples were made for each mix proportion. It should be highlighted that, in order to obtain a homogeneous mixture, the cement, supplementary cementitious materials (silica fume and fly ash), and aggregates (silica sand and iron ore) were firstly mixed for 5 min. Meanwhile, the GSNSs solution was mixed with superplasticizer, stirring evenly, and poured in part of the water, stirring evenly once again. After that the mixed solution was added to these dry materials and mixed in the mixer for another 5 min. Note that the rest of water was firstly used to flush the mixed solution container, before it was added to the mixer.

### 2.3. Testing methods

#### 2.3.1. Mechanical properties

To study the influence of GSNSs on mechanical performance of ferro-siliceous sacrificial cement paste and mortar, both flexural and compressive strength of ferro-siliceous sacrificial cement paste and mortar with different contents of GSNSs were tested according to GB/T 17617-2007 [50].

#### 2.3.2. Microstructure

A 3D environmental scanning electronic microscopy (ESEM) was used to detect the microstructural evolution in ferro-siliceous sacrificial mortar with different contents of GSNSs.

#### 2.3.3. Porosity

The AutoPore IV mercury intrusion porosimetry (MIP) produced by Micromeritics was undertaken to identify the porosity and pore size distribution of ferro-siliceous sacrificial mortar with different contents of GSNSs so as to investigate the effect of GSNSs on porosity and pore size distribution of ferro-siliceous sacrificial cement paste and mortar in a quantitative manner.

#### 2.3.4. Thermal conductivity

According to the standard ASTM E 1461–13, the thermal conductivity of ferro-siliceous sacrificial mortar with different contents of GSNSs was measured by a laser constant analyser (NETZSCH LFA457).

#### 2.3.5. Thermal analysis

The mass and enthalpy evolution of ferro-siliceous sacrificial cement paste and mortar during elevated temperature exposure were characterized by TGA and DSC techniques, respectively. The specimens were heated from ambient temperature to 1300 °C with the heating rate of 10 °C/min in nitrogen atmosphere.

#### 2.3.6. Ablation rate

Based on heat transfer theory, the relationship between ablation rate  $v_a$  and heat flux  $\dot{H}$  of ferro-siliceous sacrificial cement paste and mortar is expressed as follows,

$$v_a = \frac{\dot{H}}{\rho \cdot S \cdot \Delta E} \quad (1)$$

where  $\rho$  is the density;  $S$  is the ablating area;  $\Delta E$  is the decomposition enthalpy.

The enthalpy of ferro-siliceous sacrificial cement paste and mortar was obtained from the integration of their DSC curves [51], and the starting point of the integration was 25 °C in this work. The decomposition temperature of ferro-siliceous sacrificial cement paste and mortar was determined by a furnace at the heating rate of 5 °C/min, and then the decomposition enthalpy of ferro-siliceous sacrificial cement paste and mortar could be determined. Consequently, a quantitative analysis of the ablation rate of ferro-siliceous sacrificial cement paste and mortar was carried out.

It should be highlighted that at least three repeated experiments were tested on the flexural strength, porosity, TGA, DSC, and thermal conductivity of ferro-siliceous sacrificial cement paste and mortar so as to verify the experimental results. In addition, six replicated experiments were carried for the compressive strength of ferro-siliceous sacrificial cement paste and mortar. The data reported herein were the average values of the experimental results.

## 3. Results and discussion

### 3.1. Mechanical performance

#### 3.1.1. Flexural strength

Fig. 3 shows the flexural strength of ferro-siliceous sacrificial cement paste and mortar with different contents of GSNSs at various curing ages. As seen in Fig. 3a, the flexural strength of ferro-siliceous sacrificial cement paste increased with the increase of curing age. The flexural strength of FP1, FP2, and FP3 was lower than that of FP at the curing age of 1 day, which indicates that the addition of GSNSs led to the decrease in the flexural strength of ferro-siliceous sacrificial cement paste at a very early age

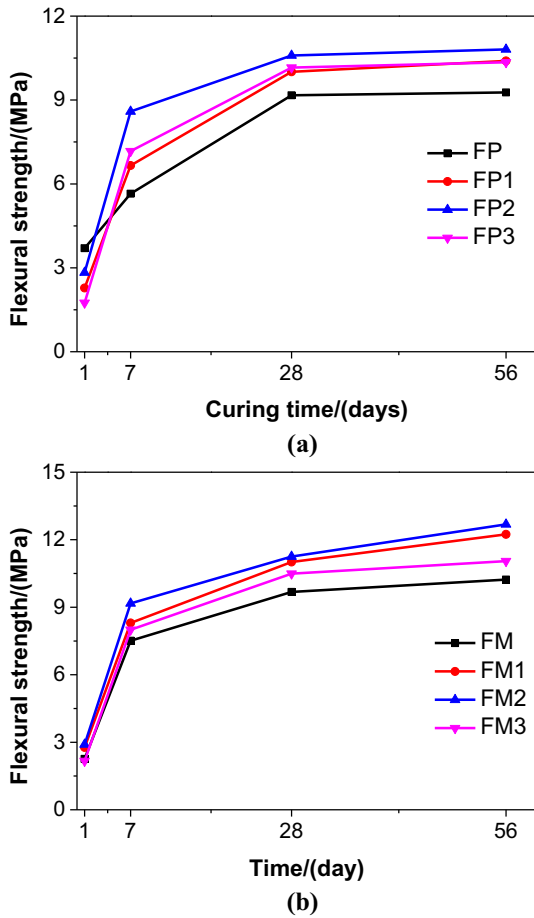


**Fig. 3.** Flexural strength of ferro-siliceous sacrificial cement paste and mortar at different curing time: (a) ferro-siliceous sacrificial cement paste; and (b) ferro-siliceous sacrificial mortar.

(1 day). The reduction caused by GSNSs was mainly due to the adsorption of their molecules on nucleating hydrate particles, which inhibited the early hydration and degree of cement. However, the flexural strength of FP1, FP2, and FP3 was always higher than that of FP at curing ages of 7, 28, and 56 days, which suggests that the flexural strength of ferro-siliceous sacrificial cement paste was improved because of the incorporation of GSNSs. The flexural strength of FP, FP1, FP2, and FP3 at the curing age of 28 days, was 9.17, 10.01, 10.59, and 10.16 MPa, respectively, which followed the sequence: FP2 > FP3 > FP1 > FP. This indicates the flexural strength of ferro-siliceous sacrificial cement paste was increased by 9.16%, 15.49%, and 10.51%, when adding 0.03 wt%, 0.1 wt%, and 0.3 wt% GSNSs, respectively.

As presented in Fig. 3b, the flexural strength of ferro-siliceous sacrificial mortar also increased with increasing curing age, which was similar to the flexural strength of ferro-siliceous sacrificial cement paste. The flexural strength of FM1 and FM2 was higher than that of FM, but the flexural strength of FM3 was lower than that of FM at the curing age of 1 day. At curing ages of 7, 28, and 56 days, the flexural strength of FM1, FM2, and FM3 was invariably higher than that of FM, following a sequence: FM2 > FM1 > FM3 > FM. This indicates that the flexural strength of ferro-siliceous sacrificial mortar could be enhanced owing to the incorporation of GSNSs. The 28-day flexural strength of FM, FM1, FM2, and FM3, was 9.68, 11.01, 11.25, and 10.49 MPa, respectively, which means the flexural strength of ferro-siliceous sacrificial mortar was increased by 13.74%, 16.22%, and 8.37%, if 0.03 wt%, 0.1 wt%, and 0.3 wt% GSNSs were added, respectively.

To sum up, the flexural strength of ferro-siliceous sacrificial cement paste and mortar at an early curing age (1 day) was decreased because of the incorporation of GSNSs, while the flexural strength of ferro-siliceous sacrificial cement paste and mortar was increased by 15.49% (FP2) and 16.22% (FM2) at the curing age of 28 days, respectively, when adding 0.1 wt% GSNSs. These findings indicate that the GSNSs have the same function as the GNS and GONSs, and can improve the flexural strength of cementitious materials.

### 3.1.2. Compressive strength

Fig. 4 presents the compressive strength of ferro-siliceous sacrificial cement paste and mortar with different contents of GSNSs at various curing ages is shown in. Along with the increase of curing age, the compressive strength of ferro-siliceous sacrificial cement paste increased (see Fig. 4a). The compressive strength of FP1, FP2, and FP3 was always higher than that of FP at each curing age, which demonstrates that the compressive strength of ferro-siliceous sacrificial cement paste was improved because of the addition of GSNSs. The compressive strength of FP, FP1, FP2, and FP3 at the curing age of 28 days, was 69.27, 70.75, 74.62, and 70.99 MPa, respectively, following a sequence: FP2 > FP3 > FP1 > FP, which indicates that the compressive strength of ferro-siliceous sacrificial cement paste rose by 2.14%, 7.72%, and 2.48%, when adding 0.03 wt%, 0.1 wt%, and 0.3 wt% GSNSs, respectively. It should be noted that the experimental result suggested that the compressive strength of ferro-siliceous sacrificial cement paste was slightly improved due to the addition of GSNSs.

The compressive strength of ferro-siliceous sacrificial mortar also increased as curing age increased (see Fig. 4b), which is similar to the compressive strength of ferro-siliceous sacrificial cement paste. The compressive strength of FM1, FM2, and FM3 was invariably lower than that of FM at the curing age of 1 day, which

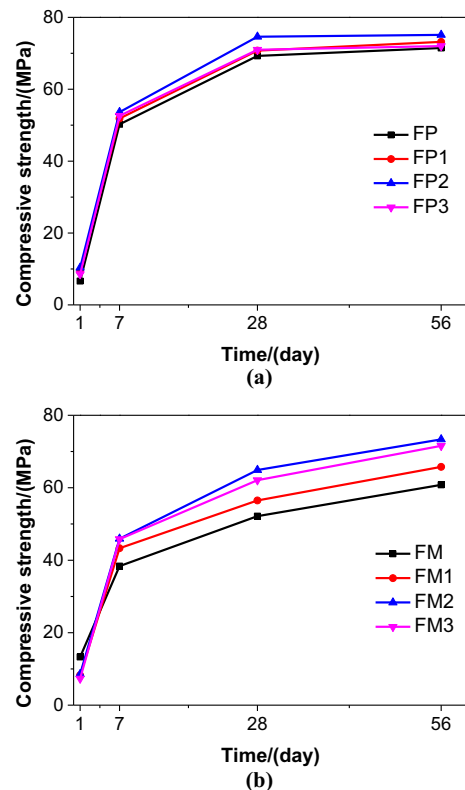


**Fig. 4.** Compressive strength of ferro-siliceous sacrificial cement paste and mortar at different curing time: (a) ferro-siliceous sacrificial cement paste; and (b) ferro-siliceous sacrificial mortar.

indicates that the 1-day compressive strength of ferro-siliceous sacrificial mortar was decreased because of the incorporation of GSNSs. Nevertheless, at curing ages of 7, 28, and 56 days, the compressive strength of FM1, FM2, and FM3 was always higher than that of FM, which suggests that the compressive strength of sacrificial mortar was improved due to the addition of GSNSs. The compressive strength of FM, FM1, FM2, and FM3 at the curing age of 28 days, was 52.16, 56.49, 64.91, and 62.10 MPa, respectively, which followed the sequence: FM2 > FM3 > FM1 > FM. This indicates that the compressive strength of ferro-siliceous sacrificial mortar was increased by 8.30%, 24.44%, and 19.06%, if 0.03 wt%, 0.1 wt%, and 0.3 wt% GSNSs were added, respectively.

Accordingly, Owing to the addition of GSNSs, the compressive strength of ferro-siliceous sacrificial cement paste and mortar at an early curing age (1 day) might be decreased, while the 28-day compressive strength of ferro-siliceous sacrificial cement paste and mortar was increased by 7.72% (FP2) and 24.44% (FM2), respectively, when 0.1 wt% GSNSs were added. These experimental results indicate that the GSNSs have the same function as the GNS and GONSs, and can enhance the compressive strength of cementitious materials.

In summary, the mechanical properties (e.g. flexural strength, compressive strength) of ferro-siliceous sacrificial cement paste and mortar was improved by adding GSNSs, and the optimal amount of GSNSs was found to be 0.1 wt% for ferro-siliceous sacrificial cement paste and mortar. Because of the incorporation of 0.1 wt% GSNSs, the flexural strength of ferro-siliceous sacrificial cement paste and mortar was increased by 15.49% (FP2) and 16.22% (FM2), respectively, and the compressive strength of ferro-siliceous sacrificial cement paste and mortar was increased by 7.72% (FP2) and 24.44% (FM2), respectively.

### 3.2. Microstructure

Fig. 5 shows the ESEM images of FM, FM1, FM2, and FM3 at curing age of 28 days. It can be seen in Fig. 5a that there were some holes, even small cracks, and loose structure in the matrix of FM. However, the matrix of FM1 was more compact than that of FM due to the addition of GSNSs. The matrix of FM2 exhibited a dense microstructure, and some cluster crystals can be observed. Some cumulate plate-shaped products were also detected, as shown in the blue square in Fig. 5c. These cumulate plate-shaped products might have enhancing effects on microstructure of ferro-siliceous sacrificial mortar. The enlarged view of cumulate plate-shaped products (see Fig. 5c) was illustrated in Fig. 5e, and the EDS analysis was carried out on the plate-shaped products. The main elemental compositions of this area were C, O, Ca, and S, the mass fractions of which were 49.27%, 30.45%, 9.74%, and 7.12%, respectively. EDS experimental results suggest that the added GSNSs resulted in the formation of cumulate plate-shaped products, because the  $-\text{SO}_3\text{H}$  in GSNSs reacted with cement hydration products [52]. It should be highlighted that the flower-like crystals was observed in the micro crack of FM3, as presented in Fig. 5d, and shown in detail in Fig. 5f, and the EDS analysis was also carried out on the flower-like crystals. The main elemental compositions of the flower-like crystals were also C, O, Ca, and S, and the mass fractions of the elements were 51.36%, 28.93%, 10.52%, and 4.98%, respectively, which indicated that the flower-like crystals were correlated with the added GSNSs. The crack-arresting and bridging effect of graphene oxide in cement paste has already been verified by Gong et al. [53]. Therefore, it was expected that the GSNSs could arrest and bridge cracks in the cement matrix like graphene oxide does. Consequently, the microstructure of ferro-siliceous sacrificial mortar was improved due to the incorporation of GSNSs, since the added GSNSs have enhancing and crack-bridging effects on its

microstructure, which is similar to the effects of GONSs on microstructure of cement paste [42]. As discussed above, the addition of GSNSs led to the increase in mechanical strengths (e.g. flexural strength, compressive strength) of ferro-siliceous sacrificial cement paste and mortar, which can be explained by the enhancing and crack-bridging effects of GSNSs.

### 3.3. Porosity and pore size distribution

The porosity of FM, FM1, FM2, and FM3 at the curing age of 28 days was 8.86%, 8.53%, 8.32%, and 8.21%, respectively, as shown in Fig. 6a. The porosity of FM1, FM2, and FM3 was lower than that of FM, as the incorporation of GSNSs into ferro-siliceous sacrificial mortar had enhancing and crack-bridging effects on its microstructure (see Fig. 5e, Fig. 5f), which resulted in decreasing porosity of ferro-siliceous sacrificial mortar. Fig. 6b shows the pore size distribution of FM, FM1, FM2, and FM3 at the curing age of 28 days, in which multiple peaks can be observed. The threshold pore diameter of FM1, FM2, and FM3 was always lower than that of FM, which implies that the porosity of FM1, FM2, and FM3 was lower than that of FM. This also indicates that the pore structure of ferro-siliceous sacrificial mortar can be improved due to the addition of GSNSs. The improvement of pore structure can be ascribed to the presence of GSNSs that have nano-filler effect, enhancing effect, and crack-bridging effect.

### 3.4. Thermal conductivity

The thermal conductivity of ferro-siliceous sacrificial mortar is presented in Fig. 7. The thermal conductivity of FM, FM1, FM2, and FM3 at the curing age of 28 days was 1.06, 1.12, 1.21, and 1.25 [W/(m·K)], respectively, as shown in Fig. 7. The thermal conductivity of FM1, FM2, and FM3 was always higher than that of FM, which indicates that the thermal conductivity of ferro-siliceous sacrificial mortar was improved because of the addition of GSNSs. Compared to FM, the thermal conductivity of FM1, FM2, and FM3 was increased by 5.66%, 14.15%, and 17.92%, when 0.03 wt%, 0.1 wt%, and 0.3 wt% GSNSs were added, respectively. The microstructure of ferro-siliceous sacrificial mortar was improved due to the addition of GSNSs (see Fig. 5), which caused the decrease of discontinuous crystal boundaries in matrix, and thus the thermal conductivity of ferro-siliceous sacrificial mortar could be increased based on heat transfer theory [54]. In addition, the heat transmission resistance of ferro-siliceous sacrificial mortar with evenly distributed GSNSs could be declined due to the excellent heat conductivity of GSNSs itself, which could also improve the thermal conductivity of ferro-siliceous sacrificial mortar.

### 3.5. Thermal analysis

#### 3.5.1. Thermogravimetric analysis

The thermogravimetric analysis results of ferro-siliceous sacrificial cement paste and mortar are shown in Fig. 8. The weight evolution of ferro-siliceous sacrificial cement paste and mortar was similar, because their mix proportions were almost the same (see Table 3). The weight of ferro-siliceous sacrificial cement paste and mortar was falling quickly, when the temperature range was 25–150 °C, the result of which is in line with the findings of Ye et al. [55]. The loss of evaporable water and partial physical bounding water in ferro-siliceous sacrificial cement paste and mortar was the main cause of this phenomenon. In the range of 105–700 °C, the mass declined because of the loss of chemical bounding water and the decomposition of hydration products [56]. The weight of ferro-siliceous sacrificial cement paste and mortar was falling rapidly at approximately 700 °C due to the decomposition of

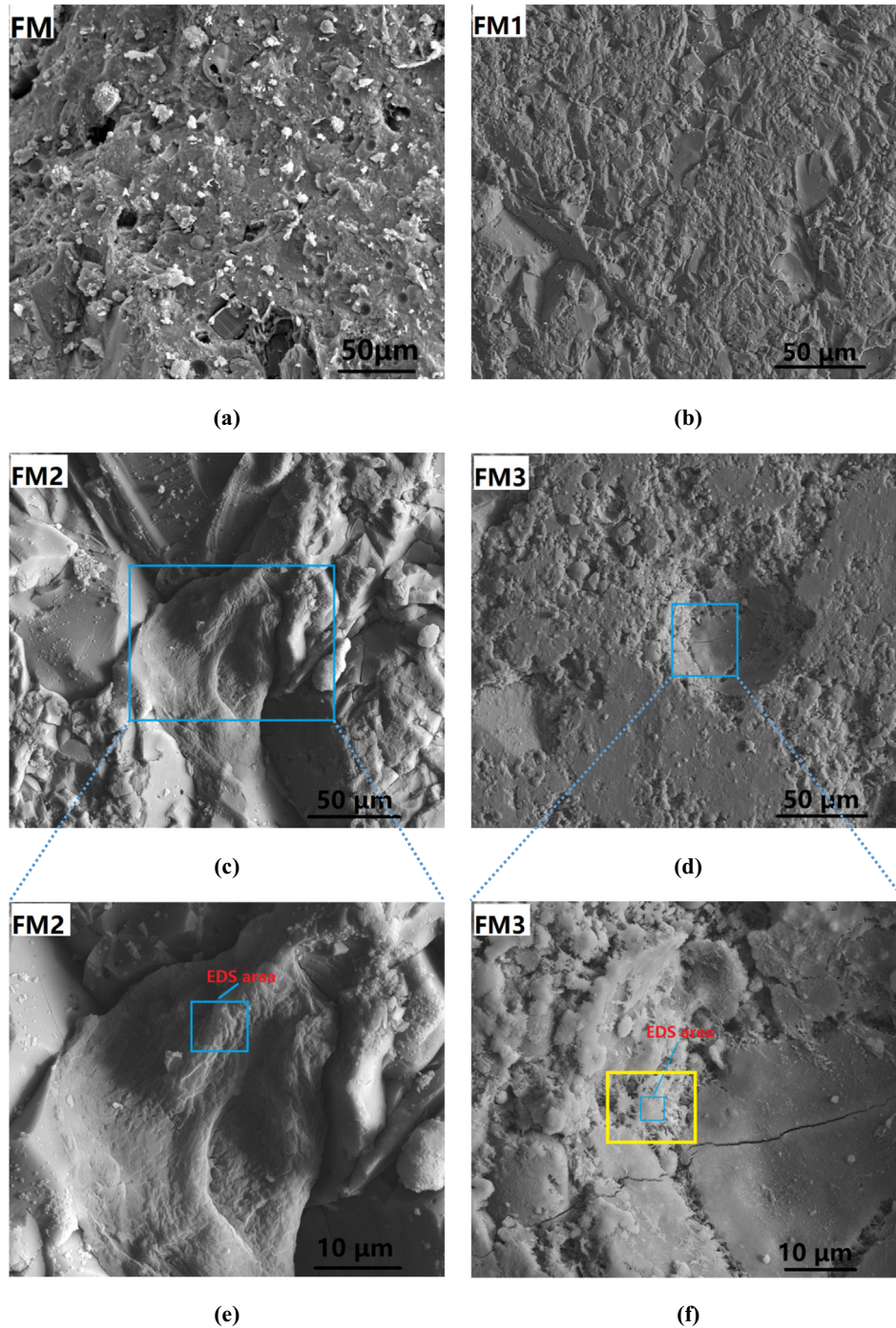


Fig. 5. ESEM micrographs of FM, FM1, FM2, and FM3 at curing time of 28 days.

$\text{CaCO}_3$ , and the curves of TGA varied slowly after this temperature. The weight of ferro-siliceous sacrificial cement paste and mortar was declining fast again at about 1200 °C, which resulted from the melting of Portland cement. The total weight loss of ferro-siliceous sacrificial cement paste up to 1300 °C was 25.50% (FP), 24.72% (FP1), 26.08% (FP2), and 25.35% (FP3), respectively. The total weight loss of ferro-siliceous sacrificial mortar up to 1300 °C was 7.36% (FM), 9.62% (FM1), 6.98% (FM2), and 9.00% (FM3), respectively. Overall, the weight loss of ferro-siliceous sacrificial cement paste up to 1300 °C was higher than that of ferro-siliceous sacrificial mortar.

### 3.5.2. Differential scanning calorimetry

Fig. 9 depicts the differential scanning calorimetry results of ferro-siliceous sacrificial cement paste and mortar. The DSC curves of ferro-siliceous sacrificial cement paste and mortar were also close, because their hydration products were roughly the same. The dehydration process of ferro-siliceous sacrificial cement paste and mortar occurred at about 100 °C, accompanied by loss of evaporable water and partial physical bounding water. This finding is in accordance with the experimental results of other researchers [56]. When the temperature range was 400–600 °C, the CH began to decompose, which is consistent with that reported in literature

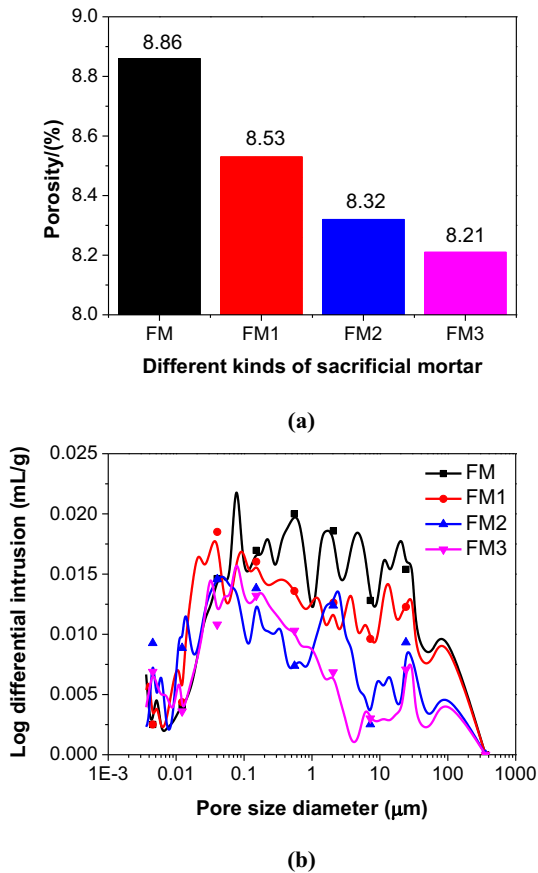


Fig. 6. Porosity and pore size distribution of FM, FM1, FM2, and FM3 at curing time of 28 days: (a) porosity; and (b) pore size distribution.

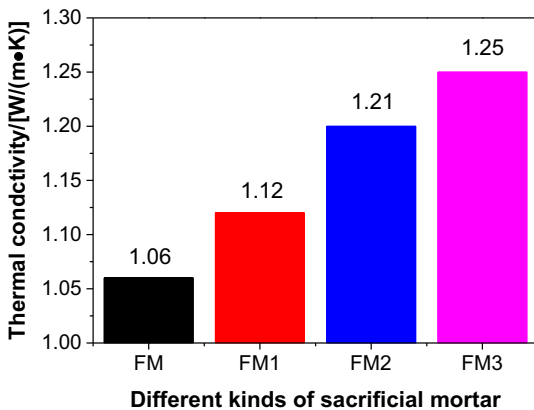


Fig. 7. Thermal conductivity of FM, FM1, FM2, and FM3 at curing time of 28 days.

[56]. The crystal phase transformation of quartz ( $\beta$ - to  $\alpha$ - quartz) went on at 580 °C or so, and this result is accordant with the published paper by Chase [51]. The  $\text{CaCO}_3$  decomposed at about 700 °C in the work, the result of which is consistent with the conclusion drawn by Bazant and Kaplan [56]. The Portland cement melted at about 1200 °C (see Fig. 9), which is also consistent with the experimental result of Chase [51]. It should be highlighted that, in general, the dehydration of hydration products was an ongoing process between 100 and 850 °C.

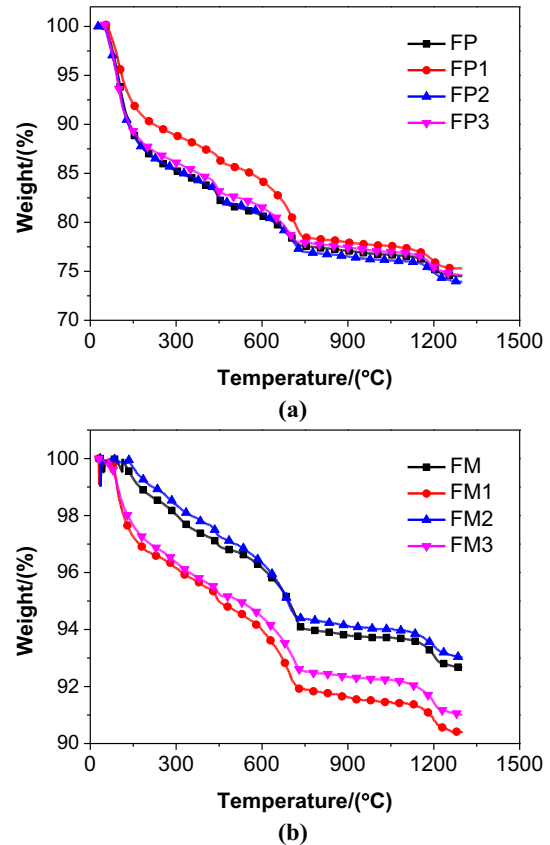


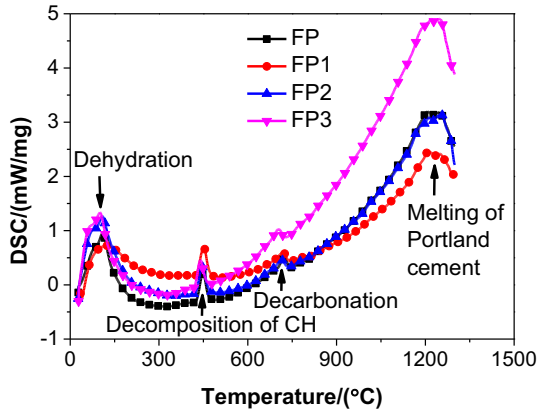
Fig. 8. Thermogravimetric analysis of ferro-siliceous sacrificial cement paste and mortar: (a) ferro-siliceous sacrificial cement paste; and (b) ferro-siliceous sacrificial mortar.

### 3.6. Ablation behaviour

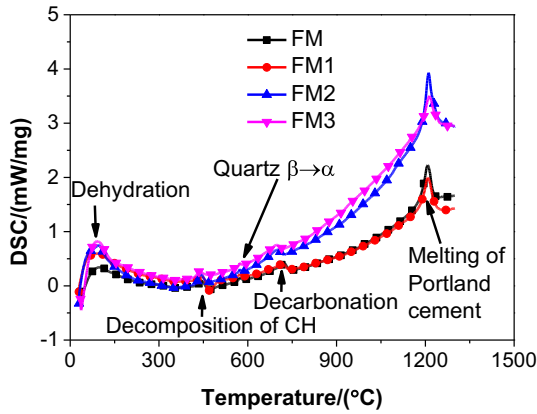
The ferro-siliceous sacrificial cement paste and mortar decomposed at the temperature range of 1200–1250 °C, based on the elevated temperature tests via the furnace. From the results plotted in Fig. 9, the enthalpy of ferro-siliceous sacrificial cement paste and mortar can be obtained and is presented in Fig. 10.

As shown in Fig. 10, the enthalpy of ferro-siliceous sacrificial cement paste and mortar increased gradually before a sharp rise, except for FP, FP2, and FP3. When the addition of GSNSs was 0 wt%, 0.03 wt%, 0.1 wt%, and 0.3 wt%, the decomposition enthalpy of ferro-siliceous sacrificial cement paste was 785.24 kJ/kg (FP), 871.10 kJ/kg (FP1), 903.42 kJ/kg (FP2), and 1648.44 kJ/kg (FP3), respectively, which indicates that the decomposition enthalpy of ferro-siliceous sacrificial cement paste increased with the increase of GSNSs. The decomposition enthalpy of ferro-siliceous sacrificial cement paste was increased by 10.93%, 15.05%, and 109.93%, when the addition of GSNSs was 0.03 wt%, 0.1 wt%, and 0.3 wt%, respectively. When adding GSNSs 0 wt%, 0.03 wt%, 0.1 wt%, and 0.3 wt%, the decomposition enthalpy of ferro-siliceous sacrificial mortar was 441.95 kJ/kg (FM), 506.69 kJ/kg (FM1), 889.76 kJ/kg (FM2), and 1039.25 kJ/kg (FM3), respectively, which suggests that the decomposition enthalpy of ferro-siliceous sacrificial mortar was increased due to the incorporation of GSNSs. When the addition of GSNSs was 0.03 wt%, 0.1 wt%, and 0.3 wt%, the decomposition enthalpy of ferro-siliceous sacrificial mortar was increased by 14.65%, 101.33%, and 135.15%, respectively.

According to Eq. (1), the ablation rate is proportionate to the heat flux, however it is inversely in proportion to its decomposition



(a)



(b)

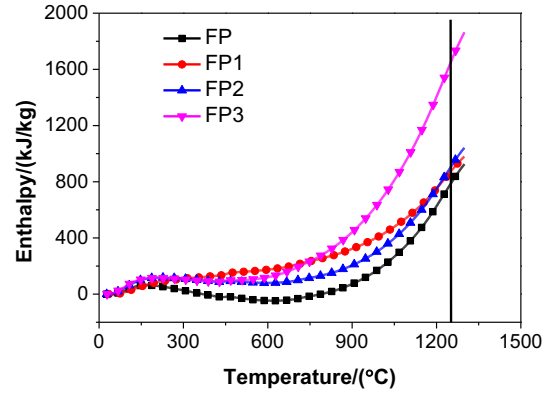
**Fig. 9.** Differential scanning calorimetry results of ferro-siliceous sacrificial cement paste and mortar: (a) ferro-siliceous sacrificial cement paste; and (b) ferro-siliceous sacrificial mortar.

enthalpy, when ablating area and density remains constant. Hence, the ablation rate of ferro-siliceous sacrificial cement paste and mortar was reduced due to the addition of GSNSs. The ablation rate of ferro-siliceous sacrificial cement paste was reduced by 9.85%, 13.08%, and 52.37%, when the addition of GSNSs was 0.03 wt%, 0.1 wt%, and 0.3 wt%, respectively. The ablation rate of ferro-siliceous sacrificial mortar decreased by 12.79%, 50.33%, and 57.47%, when adding GSNSs 0.03 wt%, 0.1 wt%, and 0.3 wt%, respectively. Accordingly, the ablating time of basemat sacrificial material can be extended, and then the security of nuclear power plant can be greatly improved.

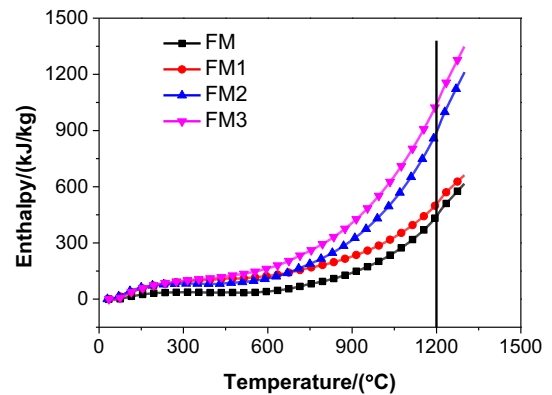
In summary, compared to ferro-siliceous sacrificial cement paste and mortar without GSNSs, the sacrificial cement paste and mortar containing GSNSs were found to have higher flexural strength, higher compressive strength, more compact matrix, lower porosity, higher decomposition enthalpy, and lower ablation rate. GSNSs can improve the microstructure and properties of ferro-siliceous sacrificial cement paste and mortar. Taking microstructure, mechanical strength, ablation rate of siliceous sacrificial cement paste and mortar into consideration, the optimal amount of GSNSs was 0.1 wt%. It is expected that these findings can contribute to designing new kind of ferro-siliceous sacrificial cement paste, mortar, and even concrete containing GSNSs.

**4. Conclusions**

In this paper, the influence of GSNSs on microstructure and properties of ferro-siliceous sacrificial cement paste and mortar



(a)



(b)

**Fig. 10.** Enthalpy and decomposition enthalpy of ferro-siliceous sacrificial cement paste and mortar: (a) ferro-siliceous sacrificial cement paste; and (b) ferro-siliceous sacrificial mortar.

with different contents of GSNSs were studied. On the basis of experimental findings, the main conclusions of the research are summarized as follows,

- (1) The mechanical strengths (e.g. flexural strength, compressive strength) of ferro-siliceous sacrificial cement paste and mortar can be improved by adding GSNSs, and the optimal amount of GSNSs is found to be 0.1 wt% in ferro-siliceous sacrificial cement paste and mortar. When adding 0.1 wt% GSNSs, the flexural strength of ferro-siliceous sacrificial cement paste and mortar is increased by 15.49% and 16.22%, respectively, and the compressive strength of ferro-siliceous sacrificial cement paste and mortar is increased by 7.72% and 24.44%, respectively.
- (2) GSNSs have enhancing effects on microstructure of ferro-siliceous sacrificial mortar, and can improve its microstructure. The porosity of ferro-siliceous sacrificial mortar is reduced because of the incorporation of GSNSs, which can be ascribed to the enhancing effect, nano-filler effect, and cracking-bridging effect of GSNSs.
- (3) The total weight loss of ferro-siliceous sacrificial cement paste up to 1300 °C is 25.50%, 24.72%, 26.08%, and 25.35%, respectively, and the total weight loss of ferro-siliceous sacrificial mortar up to 1300 °C is 7.36%, 9.62%, 6.98%, and 9.00%, respectively, when the addition of GSNSs is 0 wt%, 0.03 wt%, 0.1 wt%, and 0.3 wt%, respectively. Overall, the weight loss of ferro-siliceous sacrificial cement paste up to 1300 °C is higher than that of sacrificial mortar.

- (4) The differential scanning calorimetry patterns of ferro-siliceous sacrificial cement paste and mortar are also close, because their hydration products are roughly the same.
- (5) The thermal conductivity of ferro-siliceous sacrificial mortar is improved because of the addition of GSNSs. When the addition of GSNSs is 0.03 wt%, 0.1 wt%, and 0.3 wt%, the thermal conductivity of ferro-siliceous sacrificial mortar is increased by 5.66%, 14.15%, and 17.92%, respectively.
- (6) The decomposition enthalpy of ferro-siliceous sacrificial cement paste and mortar is increased with increasing GSNSs content. When the addition of GSNSs is 0.03 wt%, 0.1 wt%, and 0.3 wt%, the decomposition enthalpy of ferro-siliceous sacrificial cement paste is increased by 10.93%, 15.05%, and 109.93%, respectively, and the decomposition enthalpy of ferro-siliceous sacrificial mortar is increased by 14.65%, 101.33%, and 135.15%, respectively.
- (7) The ablation rate of ferro-siliceous sacrificial cement paste and mortar can be reduced, due to addition of GSNSs. When the addition of GSNSs is 0.03 wt%, 0.1 wt%, and 0.3 wt%, the ablation rate of ferro-siliceous sacrificial cement paste is reduced by 9.85%, 13.08%, and 52.37%, respectively, and the ablation rate of ferro-siliceous sacrificial mortar reduces by 12.79%, 50.33%, and 57.47%, respectively.

## Acknowledgements

The research is financially supported by the National Natural Science Foundation of China, China (No. 51808294), the Natural Science Foundation of Education Department of Jiangsu, China (general program, 18KJB430017), Jiangsu Key Laboratory of Construction Material, China (CM2018-01), Scientific Research Project of Jiangsu Provincial Department of Housing and Urban-Rural Development, China (094828867208), and the Ministry of Science and Technology of China, China (973 program, 2015CB655105), which are gratefully acknowledged.

## References

- [1] R.V. Sagar, B.K.R. Prasad, S.S. Kumar, An experimental study on cracking evolution in concrete and cement mortar by the b-value analysis of acoustic emission technique, *Cem. Concr. Res.* 42 (8) (2012) 1094–1104.
- [2] D. Carnelli, R. Libanori, B. Feichtenschlager, L. Nicoleau, G. Albrecht, A.R. Studart, Cementitious composites reinforced with localized and magnetically oriented Al<sub>2</sub>O<sub>3</sub> microplatelets, *Cem. Concr. Res.* 78 (2015) 245–251.
- [3] M. Zahedi, A.A. Ramezani-pour, A.M. Ramezani-pour, Evaluation of the mechanical properties and durability of cement mortars containing nanosilica and rice husk ash under chloride ion penetration, *Constr. Build. Mater.* 78 (2015) 354–361.
- [4] Z. Lu, D. Hou, H. Ma, T. Fan, Z. Li, Effects of graphene oxide on the properties and microstructures of the magnesium potassium phosphate cement paste, *Constr. Build. Mater.* 119 (2016) 107–112.
- [5] C. Nunes, Z. Slizkova, M. Stefanidou, J. Nemecek, Microstructure of lime and lime-pozzolana pastes with nanosilica, *Cem. Concr. Res.* 83 (2016) 152–163.
- [6] M. Nili, A. Ehsani, Investigating the effect of the cement paste and transition zone on strength development of concrete containing nanosilica and silica fume, *Mater. Des.* 75 (2015) 174–183.
- [7] P. Hou, S. Kawashima, D. Kong, D.J. Corr, J. Qian, S.P. Shah, Modification effects of colloidal nanoSiO<sub>2</sub> on cement hydration and its gel property, *Compos. Part B Eng.* 45 (2013) 440–448.
- [8] E. Ghafari, H. Costa, E. Julio, A. Portufal, L. Duraes, The effect of nanosilica addition on flowability, strength and transport properties of ultra high performance concrete, *Mater. Des.* 59 (2014) 1–9.
- [9] G. Quercia, P. Spiesz, G. Husken, H.J.H. Brouwers, SCC modification by use of amorphous nano-silica, *Cem. Concr. Compos.* 45 (2014) 69–81.
- [10] A.D. Alessandro, M. Rallini, F. Ubertini, A.L. Materazzi, J.M. Kenny, Investigation on scalable fabrication procedures for self-sensing carbon nanotube cement-matrix composites for SHM applications, *Cem. Concr. Compos.* 65 (2016) 200–213.
- [11] S. Parveen, S. Rana, R. Fanguero, M.C. Paiva, Microstructure and mechanical properties of carbon nanotube reinforced cementitious composites developed using a novel dispersion technique, *Cem. Concr. Res.* 73 (2015) 215–227.
- [12] P. Stynoski, P. Mondal, C. Marsh, Effects of silica additives on fracture properties of carbon nanotube and carbon fiber reinforced Portland cement mortar, *Cem. Concr. Compos.* 55 (2015) 232–240.
- [13] F. Azhari, N. Bantia, Cementitious sensors with carbon fibers and carbon nanotubes for piezoresistive sensing, *Cem. Concr. Compos.* 34 (2012) 866–873.
- [14] F. Collins, J. Lambert, W.H. Duan, The influence of admixtures on the dispersion, workability, and strength of carbon nanotube-OPC paste mixtures, *Cem. Concr. Compos.* 34 (2012) 201–207.
- [15] M.S. Konsta-Gdoutos, C.A. Aza, Self-sensing carbon nanotube (CNT) and nanofiber (CNF) cementitious composites for real time damage assessment in smart structures, *Cem. Concr. Compos.* 53 (2014) 162–169.
- [16] B.M. Tyson, R.K.A. Al-Rub, A. Yazadanbakhsh, Z. Graslev, Carbon nanotubes and carbon nanofibers for enhancing the mechanical properties of nanocomposite cementitious materials, *J. Mater. Civ. Eng.* 23 (2011) 1028–1035.
- [17] S. Kawashima, J.W.T. Seo, D. Corr, M.C. Hersam, S.P. Shah, Dispersion of CaCO<sub>3</sub> nanoparticles by sonication and surfactant treatment for application in fly ash-cement systems, *Mater. Struct.* 47 (2014) 1011–1023.
- [18] T. Menga, Y. Yub, X. Qiana, S. Zhana, K. Qiana, Effect of nano-TiO<sub>2</sub> on the mechanical properties of cement mortar, *Constr. Build. Mater.* 29 (2012) 241–245.
- [19] P. Krishnan, M.-H. Zhang, L. Yu, H. Feng, Photocatalytic degradation of particulate pollutants and self-cleaning performance of TiO<sub>2</sub>-containing silicate coating and mortar, *Constr. Build. Mater.* 44 (2013) 309–316.
- [20] H. Li, H. Xiao, X. Guan, Z. Wang, L. Yu, Chloride diffusion in concrete containing nano-TiO<sub>2</sub> under coupled effect of scouring, *Compos. Part B Eng.* 56 (2014) 698–704.
- [21] M.S. Konsta-Gdoutos, Z.S. Metaxa, S.P. Shah, Multi-scale mechanical and fracture characteristics and early-age strain capacity of high performance carbon nanotube/cement nanocomposites, *Cem. Concr. Compos.* 32 (2) (2010) 110–115.
- [22] M.D. Stoller, S. Park, Y. Zhu, J. An, R.S. Ruoff, Graphene-based ultracapacitors, *Nano Lett.* 8 (2008) 3498–3502.
- [23] C.G. Lee, X.D. Wei, J.W. Kysar, J. Hone, Measurement of the elastic properties and intrinsic strength of monolayer graphene, *Science* 321 (2008) 385–388.
- [24] A.K. Geim, K.S. Novoselov, The rise of graphene, *Nat. Mater.* 6 (2007) 183–191.
- [25] Y. Zhu, S. Murali, W. Cai, X. Li, J.W. Suk, J.R. Potts, R.S. Ruoff, Graphene and graphene oxide: synthesis, properties, and applications, *Adv. Mater.* 22 (2010) 3906–3924.
- [26] T. Kuilla, S. Bhadra, D. Yao, N.H. Kim, S. Bose, J.H. Lee, Recent advances in graphene based polymer composites, *Prog. Polym. Sci.* 35 (11) (2010) 1350–1375.
- [27] C. Soldano, A. Mahmood, E. Dujardin, Production, properties and potential of graphene, *Carbon* 48 (8) (2010) 2127–2150.
- [28] Z. Pan, L. He, L. Qiu, A.H. Korayem, G. Li, J.W. Zhu, F. Collins, D. Li, W.H. Duan, M. C. Wang, Mechanical properties and microstructure of a graphene oxide-cement composite, *Cem. Concr. Compos.* 58 (2015) 140–147.
- [29] V. Chabot, D. Higgins, A. Yu, X. Xiao, Z. Chen, J. Zhang, A review of graphene and graphene oxide sponge: material synthesis and applications to energy and the environment, *Energy Environ. Sci.* 7 (5) (2014) 1564–1596.
- [30] J.L. Le, H. Du, S.D. Pang, Use of 2D graphene nanoplatelets (GNP) in cement composites for structural health evaluation, *Compos. Part B Eng.* 67 (2014) 555–563.
- [31] Y. Zhu, S. Murali, W. Cai, X. Li, J.W. Suk, J.R. Potts, R.S. Ruoff, Graphene and graphene oxide: synthesis, properties, and applications, *Adv. Mater.* 22 (35) (2010) 3906–3924.
- [32] Y.J. Kwon, Y. Kim, H. Jeon, S. Cho, W. Lee, J.U. Lee, Graphene/carbon nanotube hybrid as a multi-functional interfacial reinforcement for carbon fiber-reinforced composites, *Compos. Part B Eng.* 122 (2017) 23–30.
- [33] Y. Wen, Q. Yin, H. Jia, B. Yin, X. Zhang, P. Liu, J. Wang, Q. Ji, Z. Xu, Tailoring rubber-filler interfacial interaction and multifunctional rubber nanocomposites by usage of graphene oxide with different oxidation degrees, *Compos. Part B Eng.* 124 (2017) 250–259.
- [34] M. Bulut, Mechanical characterization of Basalt/epoxy composite laminates containing graphene nanopellets, *Compos. Part B Eng.* 122 (2017) 71–78.
- [35] J. Kim, L.J. Cote, F. Kim, W. Yuan, K.R. Shull, J. Huang, Graphene oxide sheets at interfaces, *J. Am. Chem. Soc.* 132 (23) (2010) 8180–8186.
- [36] E. Shamsaei, F.B. de Souza, X. Yao, E. Benhelal, A. Akbari, W. Duan, Graphene-based nanosheets for stronger and more durable concrete: a review, *Constr. Build. Mater.* 183 (2018) 642–660.
- [37] N. Ranjbar, M. Mehrli, M. Mehrli, U.J. Alengaram, M.Z. Jumaat, Graphene nanoplatelet-fly ash based geopolymer composites, *Cem. Concr. Res.* 76 (2015) 222–231.
- [38] X. Sun, Q. Wu, J. Zhang, Y. Qing, Y. Wu, S. Lee, Rheology, curing temperature and mechanical performance of oil well cement: combined effect of cellulose nanofibers and graphene nano-platelets, *Mater. Des.* 114 (2017) 92–101.
- [39] H. Du, H. Jacy Gao, S.D. Pang, Improvement in concrete resistance against water and chloride ingress by adding graphene nanoplatelet, *Cem. Concr. Res.* 83 (2016) 114–123.
- [40] M.M. Mokhtar, S.A. Abo-El-Enin, M.Y. Hassaan, M.S. Morsy, M.H. Khalil, Mechanical performance, pore structure and micro-structural characteristics of graphene oxide nano platelets reinforced cement, *Constr. Build. Mater.* 138 (2017) 333–339.
- [41] S. Lv, Y. Ma, C. Qiu, T. Sun, J. Liu, Q. Zhou, Effect of graphene oxide nanosheets of microstructure and mechanical properties of cement composites, *Constr. Build. Mater.* 49 (2013) 121–127.

- [42] S. Lv, L. Deng, W. Yang, Q. Zhou, Y. Cui, Fabrication of polycarboxylate/graphene oxide nanosheet composites by copolymerization for reinforcing and toughening cement composites, *Cem. Concr. Compos.* 66 (2016) 1–9.
- [43] Ch.u. H-y, Chen J-k, The experimental study on the correlation of resistivity and damage for conductive concrete, *Cem. Concr. Compos.* 67 (2016) 12–19.
- [44] Z.D. Sha, S.S. Quek, Q.X. Pei, Z.S. Liu, T.J. Wang, V.B. Shenoy, Y.W. Zhang, Inverse pseudo hall-petch relation in polycrystalline graphene, *Sci. Rep.* 4 (2014) 5991.
- [45] Z.D. Sha, Q. Wan, Q.X. Pei, S.S. Quek, Z.S. Liu, Y.W. Zhang, V.B. Shenoy, On the failure load and mechanism of polycrystalline graphene by nanoindentation, *Sci. Rep.* 4 (2014) 7437.
- [46] R.J.M. Konings, T.R. Allen, R.E. Stoller, S. Yamanaka, *Comprehensive Nuclear Materials*, Elsevier, Amsterdam, 2012.
- [47] H. Chu, J. Jiang, W. Sun, M. Zhang, Mechanical and thermal properties of graphene sulfonate nanosheet reinforced sacrificial concrete at elevated temperatures, *Constr. Build. Mater.* 153 (2017) 682–694.
- [48] H. Chu, J. Jiang, W. Sun, M. Zhang, Thermal behavior of siliceous and ferro-siliceous sacrificial concrete subjected to elevated temperatures, *Mater. Des.* 95 (2016) 470–480.
- [49] H. Chu, J. Jiang, W. Sun, M. Zhang, Mechanical and physicochemical properties of ferro-siliceous concrete subjected to elevated temperatures, *Constr. Build. Mater.* 122 (2016) 743–752.
- [50] China Association for Engineering Construction Standardization, *China Architecture & Building* (in Chinese), Beijing, 2007.
- [51] M.W. Chase, *NIST-JANAF Thermochemical Tables*, Springer, Berlin, 1998.
- [52] Ch.u. H-y, Jiang J-y, W. Sun, M. Zhang, Effects of graphene sulfonate nanosheets on mechanical and thermal properties of sacrificial concrete during high temperature exposure, *Cem. Concr. Compos.* 82 (2017) 252–264.
- [53] K. Gong, Z. Pan, A.H. Korayem, L. Qiu, D. Li, F. Collins, C.M. Wang, W. Duan, Reinforcing effects of graphene oxide on Portland cement paste, *J. Mater. Civ. Eng.* 27 (2) (2015) A4014010.
- [54] T.L. Bergman, F.P. Incropera, D.P. DeWitt, A.S. Laine, *Fundamentals of Heat and Mass Transfer*, John Wiley & Sons, New York, 2011.
- [55] G. Ye, X. Liu, G. De Schutter, L. Taerwea, P. Vandevelddec, Phase distribution and microstructural changes of self-compacting cement paste at elevated temperature, *Cem. Concr. Res.* 37 (6) (2007) 978–987.
- [56] Z.P. Bazant, M.F. Kaplan, *Concrete at High Temperatures: Materials Properties and Mathematical Models*, Longman, London, 1996.